FULLY-DEVELOPED LAMINAR FLOW IN SINUSOIDAL GROOVES

by

Scott K. Thomas[1] and Richard C. Lykins

Department of Mechanical and Materials Engineering

Wright State University, Dayton, OH 45435-0001

and

Kirk L. Yerkes

Air Force Research Laboratory (PRPG)

Wright–Patterson AFB, OH 45433-7251

1 Abstract

The flow of a constant property fluid through a sinusoidal groove has been analyzed. A numerical solution of the conservation of mass and momentum equations for fully developed flow is presented. The mean velocity, volumetric flow rate and Poiseuille number are presented as functions of the groove geometry, meniscus contact angle and shear stress at the liquid-vapor interface. In addition, a semi-analytical solution for the normalized mean velocity in terms of the normalized shear stress at the meniscus is shown to agree with the numerical data quite well.

2 Nomenclature

A_l	cross-sectional area of the liquid, m^2
A_l^*	A_l/h^2
A_{lv}	area of the liquid-vapor interface, m^2
A_w	area of the groove wall, m^2
Bo	Bond number, $\rho g z_1^2/\sigma$
d^*	parameter defined in eqn. (5)
D_h	hydraulic diameter, $4A_l/P$, m
D_h^*	D_h/h
f	friction coefficient, $2\overline{\tau}/\rho\overline{v}^2$

[1]Author to whom correspondence should be addressed

g	acceleration due to gravity, m/s^2
h	groove height, m
h_l	height of liquid in the groove at the wall, m
h_l^*	h_l/h
n	coordinate normal to the liquid-vapor interface
n^*	n/h
p	pressure, N/m^2
P	wetted perimeter, m
P^*	P/h
P_{lv}	perimeter of the liquid-vapor interface, m
P_{lv}^*	P_{lv}/h
Po	Poiseuille number, fRe
R	radius of curvature of the meniscus, m
R^*	R/h
Re	Reynolds number, $\rho\overline{v}D_h/\mu$
v	y-direction velocity, m/s
$\overline{v}$	average y-direction velocity, m/s
v^*	$\mu v/h^2(-dp/dy)$
$\overline{v^*}$	dimensionless average y-direction velocity
$\overline{v_0^*}$	dimensionless average y-direction velocity when $\tau_{lv}^* = 0$
v'	$\overline{v^*}/\overline{v_0^*}$
$\dot{V}$	volumetric flow rate, $\overline{v}A_l$, m^3/s
$\dot{V}^*$	$\mu\dot{V}/[h^4(-dp/dy)]$
w	period of the sinusoidal groove, m
w^*	w/h
w_l	width of the liquid in the groove, m
w_l^*	w_l/h
x, y, z	coordinate directions
x^*	x/h
z_1	distance from the liquid-vapor interface to the groove bottom, m

z^*	z/h
β	groove aspect ratio, $w/2h$
ϵ	convergence criteria
μ	absolute viscosity, Pa-s
ρ	density, kg/m^3
σ	surface tension, N/m
τ_{lv}	shear stress at the liquid-vapor interface, N/m^2
τ^*_{lv}	$\tau_{lv}/h(-dp/dy)$
$\tau^*_{lv,0}$	dimensionless shear stress at the liquid-vapor interface when $\overline{v^*} = 0$
$\overline{\tau}$	average shear stress, $A_l(-dp/dy)/P$, N/m^2
$\overline{\tau_w}$	average shear stress at the groove wall, N/m^2
$\overline{\tau^*_w}$	$\overline{\tau_w}/h(-dp/dy)$
τ'	$\tau^*_{lv}/\tau^*_{lv,0}$
ϕ	meniscus contact angle, rad
$\phi_{\max}$	maximum meniscus contact angle, rad

3 Introduction

Isotropic materials such as quartz glass or borosilicate glass can be chemically etched to form micro-grooves for the enhancement of evaporative heat transfer in chip-level devices [1]. A typical etched profile in glass is shown in Fig. 1, where the profile is smooth instead of having sharp corners seen in the etching of crystalline materials such as silicon [2]. While many studies have been performed on sharp-cornered geometries (triangular grooves [3]–[7], rectangular grooves [8]–[10], and trapezoidal grooves [11]), very little information is available in the open literature on the flow of liquid in rounded-corner geometries. Stroes and Catton [12] compared the capillary performance of triangular and sinusoidal grooves by means of an experimental study. Two sets of grooves were machined into stainless steel test plates such that the cross-sectional areas of the grooves were equal. Strip heaters were placed under the plates to provide heat input. The test plates were placed at inclination angles of

4 and 6° and ethanol was added to the grooves until the liquid reached the lands of the grooves. The average wetted length of each set of grooves was recorded as the heat input was varied from 0 to 25 W. The study showed that the triangular grooves had a greater capillary pumping ability compared to the sinusoidal grooves with the same cross-sectional area, inclination angle, and heat input. Stroes and Catton postulated that this was due to the axial rate of change of the radius of curvature of the meniscus. Sinusoidal grooves, however, could dissipate a given heat input with a smaller wetted area than triangular grooves due to the larger wetted perimeter found with sinusoidal grooves.

The objective of the present study was to examine the fully-developed laminar flow of liquid in sinusoidal grooves. The effects of countercurrent and cocurrent vapor flow over the liquid-vapor interface were investigated by relating the liquid velocity gradient to the friction factor of the vapor. The variation of the shear stress on the liquid-vapor interface [10] was neglected, and the liquid-vapor interface was assumed to be circular (Bo $\ll 1$). The mean velocity, volumetric flow rate and Poiseuille number were determined as functions of the interfacial shear stress, the meniscus contact angle, the groove aspect ratio and the amount that the groove was filled.

4 Mathematical Model

A constant property liquid flows steadily in a sinusoidal groove as shown in Fig. 2. A meniscus, which is assumed to be circular, comprises the liquid-vapor interface. For fully developed laminar flow, the conservation of mass and momentum equations reduce to the classic Poisson equation in dimensionless form [13]

$$\frac{\partial^2 v^*}{\partial x^{*2}} + \frac{\partial^2 v^*}{\partial z^{*2}} = -1 \tag{1}$$

On the groove wall, the no-slip condition is in effect.

$$v^* = 0: \quad 0 \le x^* \le w_l^*/2, \quad z^* = \frac{1}{2}\left\{1 + \cos\left[-\pi\left(\frac{x^*}{\beta} + 1\right)\right]\right\} \tag{2}$$

At the line of symmetry, the velocity gradient is zero in the x^* direction

$$\frac{\partial v^*}{\partial x^*} = 0: \quad x^* = 0, \quad 0 \le z^* \le h_l^* + R^*\sqrt{1 - \left(\frac{w_l^*}{2R^*}\right)^2} - R^* \tag{3}$$

The dimensionless radius of curvature is given by

$$R^* = \left(\frac{w_l^*}{2}\right)\left[1 + \frac{(1 + d^* \tan\phi)^2}{(d^* - \tan\phi)^2}\right]^{\frac{1}{2}} \tag{4}$$

where

$$d^* = \frac{\pi}{2\beta}\sin\left[-\pi\left(\frac{w_l^*}{2\beta} + 1\right)\right] \tag{5}$$

The maximum value for the meniscus contact angle ϕ for a wetting fluid can be determined for a given geometry by allowing the radius of curvature to approach $R^* \to \infty$.

$$\phi_{\max} = \tan^{-1}\left\{\frac{\pi}{2\beta}\sin\left[-\pi\left(\frac{w_l^*}{2\beta} + 1\right)\right]\right\} \tag{6}$$

At the liquid-vapor interface, a uniform shear stress is imposed in the y direction.

$$\frac{\partial v^*}{\partial n^*} = \tau_{lv}^* : \ 0 \le x^* \le w_l^*/2, \ z^* = h_l^* + R^*\sqrt{1 - \left(\frac{w_l^*}{2R^*}\right)^2} - \sqrt{R^{*2} - x^{*2}} \tag{7}$$

The dimensional shear stress at the liquid-vapor interface can be cast in terms of the friction factor of the vapor.

$$\tau_{lv} = \begin{cases} \left[\dfrac{\rho_v\left(\overline{v_v}\right)^2}{2}\right] f_v & \text{for cocurrent flow} \\ -\left[\dfrac{\rho_v\left(\overline{v_v}\right)^2}{2}\right] f_v & \text{for countercurrent flow} \end{cases} \tag{8}$$

The Poiseuille number of the liquid in the groove is given by

$$\mathrm{Po} = f\mathrm{Re} = \frac{D_h^{*2}}{2\overline{v^*}} \tag{9}$$

The dimensionless hydraulic diameter for the flow of liquid in a sinusoidal groove with a circular meniscus is $D_h^* = 4A_l^*/P^*$, where the dimensionless cross-sectional area of the liquid is given by

$$\begin{aligned} A_l^* =& \frac{w_l^*}{2}(2h_l^* - 1) - R^*\left[R^*\cos^{-1}\sqrt{1 - \left(\frac{w_l^*}{2R^*}\right)^2} - \left(\frac{w_l^*}{2}\right)\sqrt{1 - \left(\frac{w_l^*}{2R^*}\right)^2}\right] \\ &+ \left(\frac{\beta}{\pi}\right)\sin\left[-\pi\left(\frac{w_l^*}{2\beta} + 1\right)\right] \quad \text{for } \phi < \phi_{\max} \end{aligned} \tag{10}$$

$$A_l^* = \frac{w_l^*}{2}\left(2h_l^* - 1\right) + \left(\frac{\beta}{\pi}\right)\sin\left[-\pi\left(\frac{w_l^*}{2\beta} + 1\right)\right] \quad \text{for } \phi = \phi_{\max} \tag{11}$$

The dimensionless wetted perimeter is given by the following integral equation.

$$P^* = 2\int_0^{w_l^*/2} \sqrt{1 + \left(\frac{\pi}{2\beta}\right)^2 \sin^2\left[-\pi\left(\frac{x^*}{\beta} + 1\right)\right]}\, dx^* \tag{12}$$

The mean velocity is defined as

$$\overline{v^*} = \frac{2}{A_l^*}\int_0^{w_l^*/2}\int_0^{z^*} v^*\, dz^*\, dx^* \tag{13}$$

5 Numerical Model

The elliptic Poisson equation given by eqn. (1) with mixed boundary conditions [eqns. (2), (3) and (7)] was solved using Gauss-Seidel iteration with a central differencing scheme and successive over-relaxation [14]. The convergence criteria for the iterative solution was set to $\epsilon = 10^{-10}$ for each case. A grid independence check was made in which the number of grids in each direction was doubled. When the value for the Poiseuille number did not change by more than 1%, grid independence was considered to be reached. The convergence criteria was then reduced by an order of magnitude while maintaining the highest number of grids. If the Poiseuille number did not change by more than 1%, the solution was considered to be independent of both grid size and ϵ. Otherwise, a grid independence check was made at the smaller value of ϵ until a converged solution was reached. The integral equation for the wetted perimeter [eqn. (12)] was integrated numerically since no closed-form solution exists.

The numerical model was tested against an existing solution in the archival literature. Shah [15] determined the friction factors for the laminar flow within ducts of various cross sections using a least-squares-matching technique. Table 1 shows the comparison of the Poiseuille number between the present solution and that given by Shah [15] for laminar flow in a family of sinusoidal ducts. The agreement is excellent, with a maximum difference of 1.1%.

6 Results and Discussion

A numerical study has been completed in which the flow of liquid in a sinusoidal groove has been solved. Figure 3 presents contour plots of the dimensionless liquid

velocity. The maximum liquid velocity increases with cocurrent shear, and decreases with countercurrent shear, as expected. For countercurrent vapor flow, a portion of the liquid flows in the $-y$ direction, which is opposite to the direction of the pressure gradient. This flow reversal shows the potential of the vapor shear to drive the mean velocity of the liquid to zero, or to completely reverse the flow, depending on the magnitude of the pressure gradient.

Figure 4 and Table 2 show the mean velocity, volumetric flow rate and Poiseuille number versus shear stress at the liquid-vapor interface for several values of the meniscus contact angle. The mean velocity increases with both τ_{lv}^* and ϕ, but is a relatively weak function of ϕ. For a given value of meniscus contact angle, the mean velocity is linear with τ_{lv}^* due to an overall force balance on the liquid. The volumetric flow rate also increases with τ_{lv}^* and ϕ, but is a much stronger function of ϕ due to the increase in the cross-sectional area of the liquid. The Poiseuille number decreases as τ_{lv}^* increases. For cocurrent vapor flow ($\tau_{lv}^* > 0$), Po decreases steadily with τ_{lv}^*. For countercurrent flow, Po increases dramatically with $-\tau_{lv}^*$ due to the mean velocity approaching zero. In general, Po increases with ϕ due to the increase in the hydraulic diameter of the liquid.

Figure 5 and Table 3 present the mean velocity, volumetric flow rate and Poiseuille number versus the groove fill ratio for several values of the groove aspect ratio. The mean velocity increases monotonically with area ratio and groove aspect ratio. The volumetric flow rate also increases with w_l^*/w^* and β, but drops off rapidly for $w_l^*/w^* < 0.5$ due to the decrease in flow area. The Poiseuille number is relatively constant for this case. For $\beta \geq 0.5$, Po decreases and then increases with area ratio. For $\beta = 0.25$, Po increases over the range of w_l^*/w^* examined.

7 Semi-Analytical Solution for $\overline{v^*}$

As seen in Fig. $4(a)$, the mean velocity is a linear function of the imposed shear stress at the liquid-vapor interface. Since a direct numerical simulation of the liquid flow field for a number of values of the shear stress is computer resource intensive, it is appropriate to seek a semi-analytical expression for $\overline{v^*}$. Figure $6(a)$ shows the

definition of the parameters involved, where the mean velocity when the shear stress is zero ($\overline{v_0^*}$) is given by the numerical solution. The value for the liquid-vapor shear for which the mean velocity is zero ($\tau_{lv,0}^*$) is given by the following force balance analysis. Figure 6(b) shows a differential element of the liquid in the groove. A force balance between the pressure drop and the shear forces at the liquid-vapor interface and at the wall results in the following relation.

$$p_y A_l - p_{y+dy} A_l + \tau_{lv} A_{lv} - \overline{\tau_w} A_w = 0 \tag{14}$$

The areas over which the shear stresses τ_{lv} and $\overline{\tau_w}$ act are $A_{lv} = P_{lv} dy$ and $A_w = P dy$, respectively. Using these areas and nondimensionalizing gives

$$A_l^* + \tau_{lv}^* P_{lv}^* - \overline{\tau_w^*} P^* = 0 \tag{15}$$

For Poiseuille flow in ducts of arbitrary cross section, and combined Couette-Poiseuille flow between flat plates, the shear stress at the wall is related to the mean velocity of the fluid by a constant (White, 1991). Therefore, in the present analysis, it is assumed that this also holds for the flow of liquid in a sinusoidal groove with an imposed shear stress at the liquid-vapor interface.

$$\overline{\tau_w^*} = C_1 \overline{v^*} \tag{16}$$

It should be noted that the constant C_1 is probably a function of the groove geometry and meniscus contact angle. However, since the objective of this analysis is to determine the liquid-vapor shear stress when the mean liquid velocity is zero, this functionality is unimportant. The perimeter of the liquid-vapor interface is

$$P_{lv}^* = 2R^* \sin^{-1}\left(\frac{w_l^*}{2R^*}\right) \tag{17}$$

Substituting these relations into the force balance equation results in the following expression for mean velocity.

$$\overline{v^*} = \frac{1}{C_1 P^*}\left[A_l^* + 2\tau_{lv}^* R^* \sin^{-1}\left(\frac{w_l^*}{2R^*}\right)\right] \tag{18}$$

The mean velocity is zero when

$$\tau^*_{lv,0} = -\frac{A^*_l}{2R^* \sin^{-1}\left(\frac{w^*_l}{2R^*}\right)} \tag{19}$$

Figure 7(a) shows the results of eqn. (19). The numerical results shown in Fig. 4(a) were extrapolated to determine the values for shear stress at the liquid-vapor interface when $\overline{v^*} = 0$. Both curves indicate that $\tau^*_{lv,0}$ increases with ϕ due to the increasing depth of liquid in the groove. The prediction given by eqn. (19) is quite good given the simplicity of the closed-form solution. The equation for the normalized mean velocity as a function of the normalized shear stress is given by

$$v' = \overline{v^*}/\overline{v^*_0} = 1 - \tau' \tag{20}$$

where $\tau' = \tau^*_{lv}/\tau^*_{lv,0}$. The semi-analytical solution for the normalized mean velocity is shown in Fig. 7(b) with the corresponding numerical data presented in Fig. 4(a). Equation (20) predicts 94% of the data to within $\pm 20\%$ over the range of meniscus contact angle examined.

8 Conclusions

Based on the results of the numerical model of the flow of liquid in a sinusoidal groove, the following conclusions have been made: For a given meniscus contact angle, the mean velocity was linear with imposed shear stress at the liquid-vapor interface. The volumetric flow rate in the groove was negligible for groove fill ratios of less than $w^*_l/w^* < 0.5$. The Poiseuille number was a strong function of the countercurrent shear stress. A semi-analytical expression was provided to approximate the mean velocity as a function of the shear stress at the liquid-vapor interface.

9 Acknowledgement

Funding for this work was provided by the Air Force Research Laboratory (PRPG) under Contract No. F33615-98-1-2844.

References

[1] J. Kirshberg, D. Liepmann and K. Yerkes, Micro-cooler for chip-level temperature control, *Proc. SAE Aerospace Power Systems Conf.,* Paper No. 1999-01-1407 (1999).

[2] N. Maluf, *An Introduction to Microelectromechanical Systems Engineering,* pp. 41-83, Artech House, Boston (2000).

[3] P. Ayyaswamy, I. Catton and D. Edwards, Capillary flow in triangular grooves, *ASME J. Appl. Mech.* **41**, 332-336 (1974).

[4] H. Ma, G. Peterson and X. Lu, The influence of vapor-liquid interactions on the liquid pressure drop in triangular microgrooves, *Int. J. Heat Mass Transfer* **37**, 2211-2219 (1994).

[5] L. Romero and F. Yost, Flow in an open channel, *J. Fluid Mech.* **322**, 109-129 (1996).

[6] L. Lin and A. Faghri, Steady-state performance of a rotating miniature heat pipe, *AIAA J. Thermophysics Heat Transfer* **11**, 513-518 (1997).

[7] J. Kolodziej, G. Musielak, M. Kaczmarek and T. Strek, Determination of free surface and gravitational flow of liquid in triangular groove, *Computational Mechanics* **24**, 110-117 (1999).

[8] G. DiCola, Soluzionne analitica, amezzo della transformata di Fourier, di un problema di fusso in un canale rettangolare, Euratom C.C.R. Ispra (Italy), C.E.T.I.S. (1968).

[9] G. Schneider and R. DeVos, Non-dimensional analysis for the heat transport capability of axially grooved heat pipes including liquid/vapor interaction, AIAA Paper No. 80-0214 (1980).

[10] D. Khrustalev and A. Faghri, Coupled liquid and vapor flow in miniature passages with micro grooves, *ASME J. Heat Transfer* **121**, 729-733 (1999).

[11] R. Hopkins, A. Faghri and D. Khrustalev, Flat miniature heat pipes with micro capillary grooves, *ASME J. Heat Transfer* **121**, 102-109 (1999).

[12] G. Stroes and I. Catton, An experimental investigation of the capillary performance of triangular versus sinusoidal channels, *ASME J. Heat Transfer* **119**, 851-853 (1997).

[13] F. White, *Viscous Fluid Flow*, 2nd edn., pp. 104-131, McGraw-Hill, New York (1991).

[14] D. Anderson, J. Tannehill and R. Pletcher, *Computational Fluid Mechanics and Heat Transfer*, pp. 87-169, Hemisphere, New York (1984).

[15] R. Shah, Laminar flow friction and forced convection heat transfer in ducts of arbitrary geometry, *Int. J. Heat Mass Transfer* **18**, 849-862 (1975).

Table 1: Poiseuille number versus sinusoidal duct aspect ratio: Comparison of the present solution with that given by Shah (1975).

	Poiseuille Number, Po	
β	Shah (1975)	Present
1/4	14.553	14.479
1/3	14.022	13.931
1/2	13.023	12.935
$1/\sqrt{3}$	12.630	12.543
2/3	12.234	12.148
1	11.207	11.115
2	10.123	10.061
4	9.743	9.6373

Table 2: Mean velocity, Poiseuille number and volumetric flow rate versus shear stress at the liquid-vapor interface for various values of meniscus contact angle ($\beta = 0.5$, $w_l^*/2 = 0.25$, $P^* = 1.15245$).

ϕ	τ_{lv}^*	$\overline{v^*}$	Po	$\dot{V}^*$
0°	-0.1	0.18878×10^{-2}	27.088	0.17394×10^{-3}
0°	-0.075	0.26896×10^{-2}	19.013	0.24782×10^{-3}
0°	-0.05	0.35104×10^{-2}	14.567	0.32344×10^{-3}
0°	-0.025	0.43465×10^{-2}	11.765	0.40048×10^{-3}
0°	0.0	0.51353×10^{-2}	9.9581	0.47316×10^{-3}
0°	0.0625	0.71345×10^{-2}	7.1676	0.65738×10^{-3}
0°	0.125	0.91525×10^{-2}	5.5873	0.84330×10^{-3}
0°	0.25	0.13188×10^{-1}	3.8774	0.12152×10^{-2}
0°	0.375	0.17224×10^{-1}	2.9689	0.15870×10^{-2}
0°	0.5	0.21260×10^{-1}	2.4053	0.19589×10^{-2}
0°	0.75	0.29332×10^{-1}	1.7434	0.27026×10^{-2}
0°	1.0	0.37404×10^{-1}	1.3672	0.34464×10^{-2}
0°	2.0	0.69691×10^{-1}	0.73377	0.64214×10^{-2}
25°	-0.1	0.32506×10^{-2}	27.245	0.39414×10^{-3}
25°	-0.075	0.41572×10^{-2}	21.303	0.50408×10^{-3}
25°	-0.05	0.50437×10^{-2}	17.559	0.61158×10^{-3}
25°	-0.025	0.59348×10^{-2}	14.923	0.71962×10^{-3}
25°	0.0	0.68259×10^{-2}	12.974	0.82768×10^{-3}
25°	0.0625	0.90536×10^{-2}	9.7820	0.10978×10^{-2}
25°	0.125	0.11229×10^{-1}	7.8870	0.13616×10^{-2}
25°	0.25	0.15650×10^{-1}	5.6588	0.18977×10^{-2}
25°	0.375	0.20072×10^{-1}	4.4123	0.24338×10^{-2}
25°	0.5	0.24493×10^{-1}	3.6158	0.29700×10^{-2}
25°	0.75	0.33336×10^{-1}	2.6566	0.40422×10^{-2}
25°	1.0	0.42179×10^{-1}	2.0997	0.51144×10^{-2}
25°	2.0	0.77551×10^{-1}	1.1420	0.94034×10^{-2}

Table 2: cont., Mean velocity, Poiseuille number and volumetric flow rate versus shear stress at the liquid-vapor interface for various values of meniscus contact angle ($\beta = 0.5$, $w_l^*/2 = 0.25$, $P^* = 1.15245$).

ϕ	τ_{lv}^*	$\overline{v^*}$	Po	$\dot{V}^*$
50°	-0.1	0.45097×10^{-2}	27.149	0.64296×10^{-3}
50°	-0.075	0.54643×10^{-2}	22.406	0.77904×10^{-3}
50°	-0.05	0.64189×10^{-2}	19.074	0.91514×10^{-3}
50°	-0.025	0.73345×10^{-2}	16.693	0.10457×10^{-2}
50°	0.0	0.82746×10^{-2}	14.796	0.11797×10^{-2}
50°	0.0625	0.10625×10^{-1}	11.523	0.15148×10^{-2}
50°	0.125	0.12975×10^{-1}	9.4363	0.18498×10^{-2}
50°	0.25	0.17586×10^{-1}	6.9621	0.25072×10^{-2}
50°	0.375	0.22255×10^{-1}	5.5014	0.31728×10^{-2}
50°	0.5	0.26922×10^{-1}	4.5477	0.38382×10^{-2}
50°	0.75	0.36256×10^{-1}	3.3769	0.51690×10^{-2}
50°	1.0	0.45590×10^{-1}	2.6855	0.64998×10^{-2}
50°	2.0	0.82926×10^{-1}	1.4764	0.11823×10^{-1}
72.34°	-0.1	0.54127×10^{-2}	28.188	0.86146×10^{-3}
72.34°	-0.075	0.64152×10^{-2}	23.783	0.10210×10^{-2}
72.34°	-0.05	0.74177×10^{-2}	20.569	0.11805×10^{-2}
72.34°	-0.025	0.84202×10^{-2}	18.120	0.13401×10^{-2}
72.34°	0.0	0.94227×10^{-2}	16.192	0.14996×10^{-2}
72.34°	0.0625	0.11929×10^{-1}	12.790	0.18985×10^{-2}
72.34°	0.125	0.14354×10^{-1}	10.629	0.22844×10^{-2}
72.34°	0.25	0.19309×10^{-1}	7.9016	0.30730×10^{-2}
72.34°	0.375	0.24264×10^{-1}	6.2880	0.38618×10^{-2}
72.34°	0.5	0.29219×10^{-1}	5.2217	0.46504×10^{-2}
72.34°	0.75	0.39129×10^{-1}	3.8992	0.62276×10^{-2}
72.34°	1.0	0.49039×10^{-1}	3.1112	0.78048×10^{-2}
72.34°	2.0	0.88244×10^{-1}	1.7290	0.14044×10^{-1}

Table 3: Wetted perimeter, mean velocity, Poiseuille number and volumetric flow rate versus groove fill ratio for various values of groove aspect ratio ($\tau_{lv}^* = 0.0$, $\phi = 0°$).

β	w_l^*/w^*	P^*	$\overline{v^*}$	Po	$\dot{V}^*$
0.25	0.1	0.0731191	0.13005×10^{-4}	8.4006	0.35142×10^{-8}
0.25	0.2	0.223950	0.20221×10^{-3}	9.6365	0.70676×10^{-6}
0.25	0.3	0.450806	0.63058×10^{-3}	11.141	0.84242×10^{-5}
0.25	0.4	0.734032	0.12616×10^{-2}	12.059	0.40386×10^{-4}
0.25	0.5	1.04707	0.20592×10^{-2}	12.514	0.12238×10^{-3}
0.25	0.6	1.36011	0.29299×10^{-2}	12.849	0.27336×10^{-3}
0.25	0.7	1.64333	0.38585×10^{-2}	12.871	0.49958×10^{-3}
0.25	0.8	1.87019	0.47149×10^{-2}	12.940	0.77004×10^{-3}
0.25	0.9	2.02102	0.55519×10^{-2}	13.346	0.10799×10^{-2}
0.25	0.999	2.09364	0.74536×10^{-2}	15.203	0.18573×10^{-2}
0.5	0.1	0.114187	0.35380×10^{-5}	9.4469	0.82578×10^{-9}
0.5	0.2	0.288528	0.19851×10^{-3}	8.4052	0.82718×10^{-6}
0.5	0.3	0.531454	0.10922×10^{-2}	8.7511	0.20062×10^{-4}
0.5	0.4	0.827649	0.28055×10^{-2}	9.3706	0.13311×10^{-3}
0.5	0.5	1.15245	0.51353×10^{-2}	9.9581	0.47316×10^{-3}
0.5	0.6	1.47724	0.78593×10^{-2}	10.398	0.11735×10^{-2}
0.5	0.7	1.77344	0.10755×10^{-1}	10.780	0.22962×10^{-2}
0.5	0.8	2.01636	0.13817×10^{-1}	11.282	0.38892×10^{-2}
0.5	0.9	2.19070	0.17762×10^{-1}	12.443	0.64680×10^{-2}
0.5	0.999	2.30389	0.25467×10^{-1}	14.698	0.12692×10^{-1}
0.75	0.1	0.160025	0.11137×10^{-5}	10.092	0.21124×10^{-9}
0.75	0.2	0.367435	0.10959×10^{-3}	8.9207	0.44516×10^{-6}
0.75	0.3	0.634966	0.93568×10^{-3}	8.4299	0.18655×10^{-4}
0.75	0.4	0.951588	0.31271×10^{-2}	8.5312	0.17184×10^{-3}
0.75	0.5	1.29509	0.67001×10^{-2}	8.8579	0.74738×10^{-3}
0.75	0.6	1.63860	0.11328×10^{-1}	9.2444	0.21238×10^{-2}
0.75	0.7	1.95522	0.16731×10^{-1}	9.7209	0.46642×10^{-2}
0.75	0.8	2.22275	0.23143×10^{-1}	10.489	0.89608×10^{-2}
0.75	0.9	2.43016	0.32404×10^{-1}	11.885	0.17278×10^{-1}
0.75	0.999	2.58868	0.47659×10^{-1}	13.997	0.35626×10^{-1}
1.0	0.1	0.207697	0.45992×10^{-6}	10.367	0.73744×10^{-10}
1.0	0.2	0.453879	0.59860×10^{-4}	9.4362	0.22830×10^{-6}
1.0	0.3	0.752420	0.66244×10^{-3}	8.7481	0.13415×10^{-4}
1.0	0.4	1.09559	0.27276×10^{-2}	8.4926	0.16081×10^{-3}
1.0	0.5	1.46369	0.67927×10^{-2}	8.5590	0.84758×10^{-3}
1.0	0.6	1.83180	0.12785×10^{-1}	8.8427	0.27842×10^{-2}
1.0	0.7	2.17497	0.20665×10^{-1}	9.3068	0.69688×10^{-2}
1.0	0.8	2.47351	0.31143×10^{-1}	10.106	0.15279×10^{-1}
1.0	0.9	2.71969	0.46597×10^{-1}	11.485	0.32778×10^{-1}
1.0	0.999	2.92539	0.69923×10^{-1}	13.281	0.69692×10^{-1}

10 Figure Captions

1. Grooves chemically etched in glass (Courtesy of D. Liepmann, University of California at Berkeley).

2. Flow of liquid in a sinusoidal groove: (a) Definition of geometric parameters; (b) Dimensionless solution domain.

3. Dimensionless velocity fields for laminar flow in a sinusoidal groove ($\beta = 0.5$, $w_l^*/2 = 0.25$, $\phi = 25°$): (a) $\tau_{lv}^* = 2.0$ (cocurrent flow); (b) $\tau_{lv}^* = 0.0$; (c) $\tau_{lv}^* = -0.1$ (countercurrent flow).

4. Variation of the flow variables with shear stress at the liquid-vapor interface for various values of meniscus contact angle ($\beta = 0.5$, $w_l^*/2 = 0.25$, $P^* = 1.15245$): (a) Mean velocity; (b) Volumetric flow rate; (c) Poiseuille number.

5. Variation of the flow variables with groove fill ratio for various values of groove aspect ratio ($\tau_{lv}^* = 0.0$, $\phi = 0°$): (a) Mean velocity; (b) Volumetric flow rate; (c) Poiseuille number.

6. Semi-analytical solution for $\overline{v^*}$: (a) Definition of parameters; (b) Force balance on the liquid in a sinusoidal groove.

7. Comparison of the semi-analytical solution with numerical data ($\beta = 0.5$, $w_l^*/2 = 0.25$): (a) Countercurrent vapor shear stress required for $\overline{v^*} = 0$; (b) Normalized mean velocity versus normalized shear stress at the liquid-vapor interface.

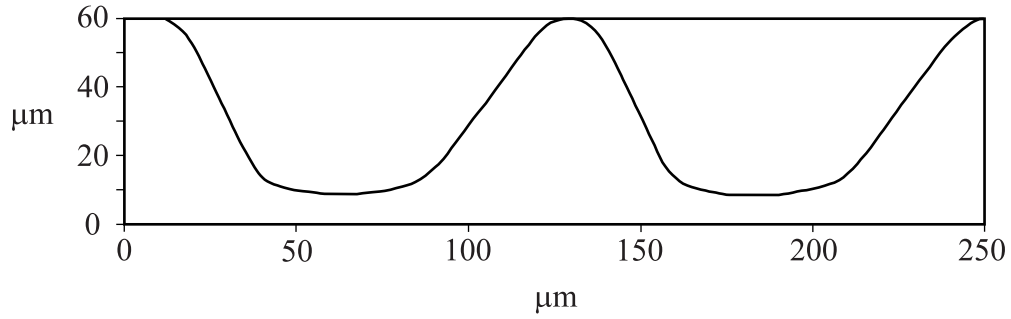

Figure 1: Grooves chemically etched in glass (Courtesy of D. Liepmann, University of California at Berkeley).

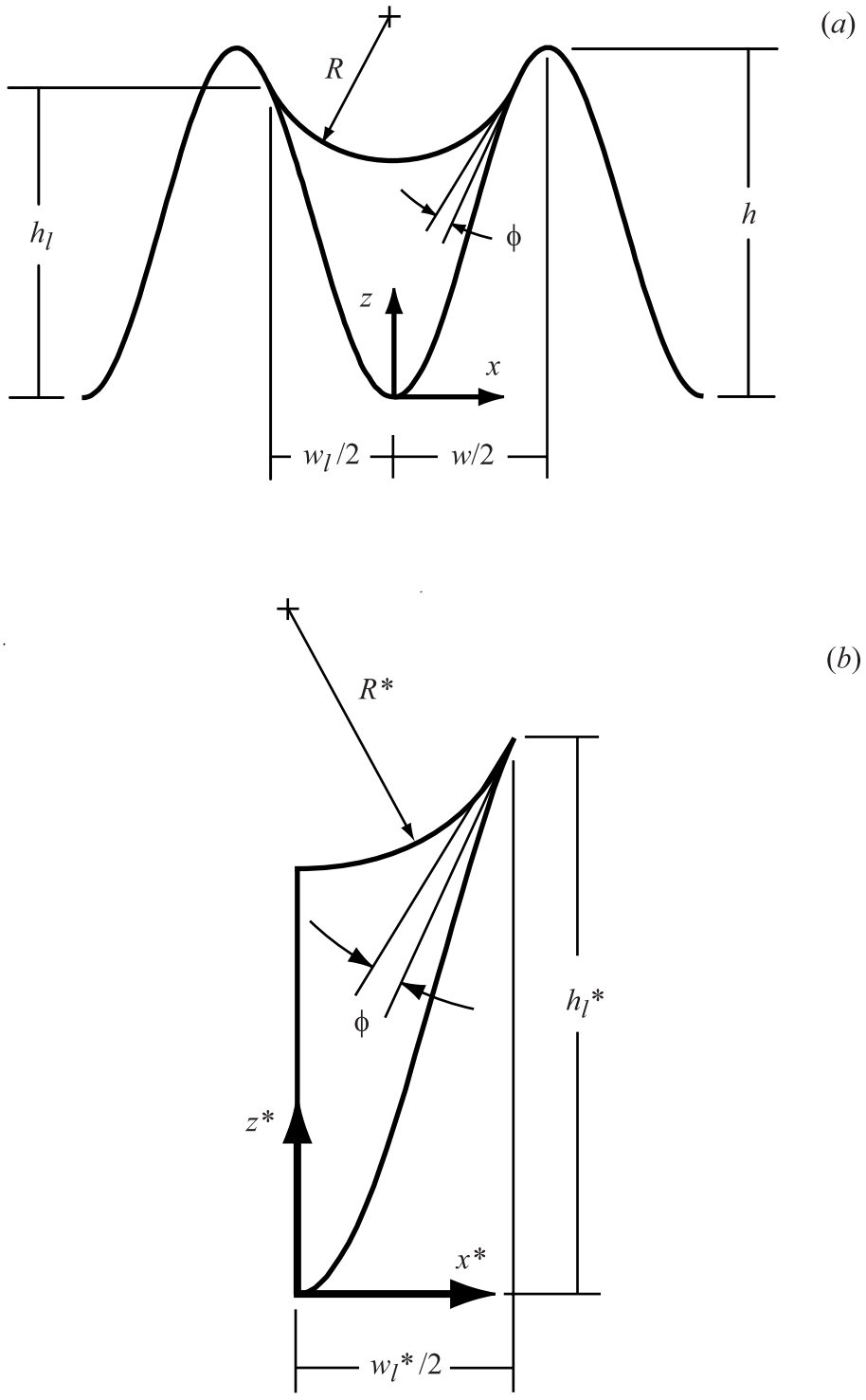

Figure 2: Flow of liquid in a sinusoidal groove: (a) Definition of geometric parameters; (b) Dimensionless solution domain.

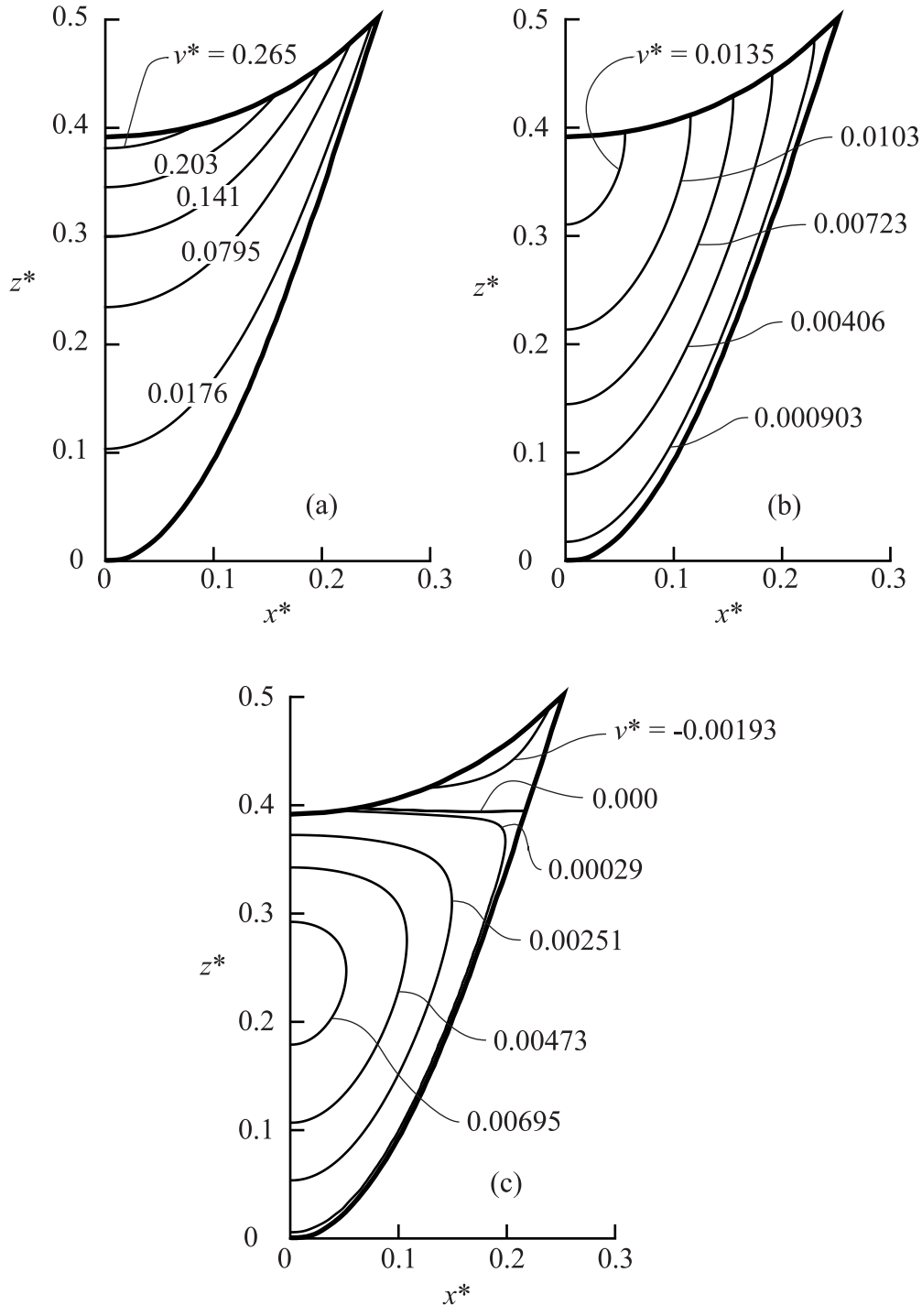

Figure 3: Dimensionless velocity fields for laminar flow in a sinusoidal groove ($\beta = 0.5$, $w_l^*/2 = 0.25$, $\phi = 25°$): (a) $\tau_{lv}^* = 2.0$ (cocurrent flow); (b) $\tau_{lv}^* = 0.0$; (c) $\tau_{lv}^* = -0.1$ (countercurrent flow).

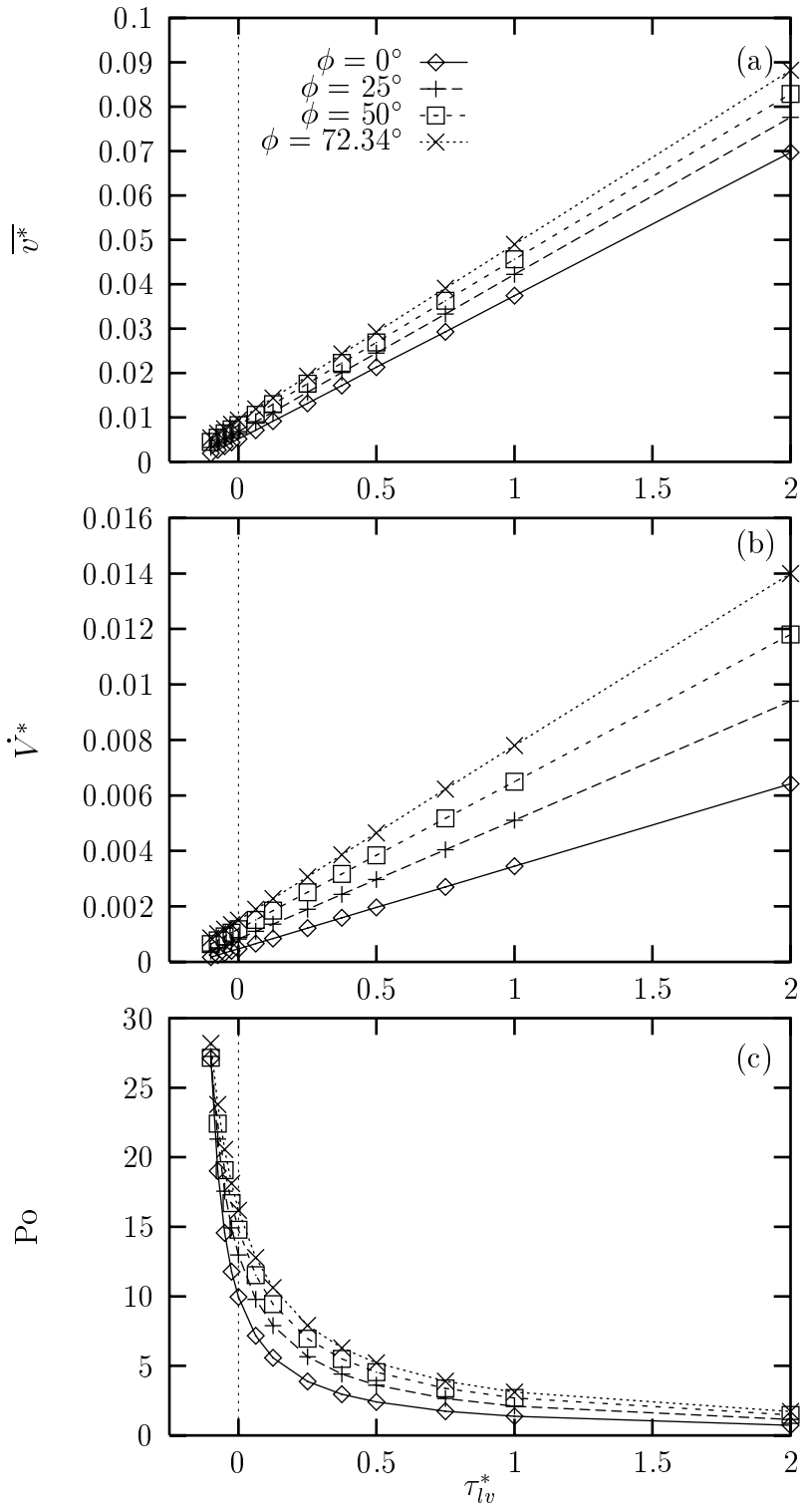

Figure 4: Variation of the flow variables with shear stress at the liquid-vapor interface for various values of meniscus contact angle ($\beta = 0.5$, $w^*_l/2 = 0.25$, $P^* = 1.15245$): (a) Mean velocity; (b) Volumetric flow rate; (c) Poiseuille number.

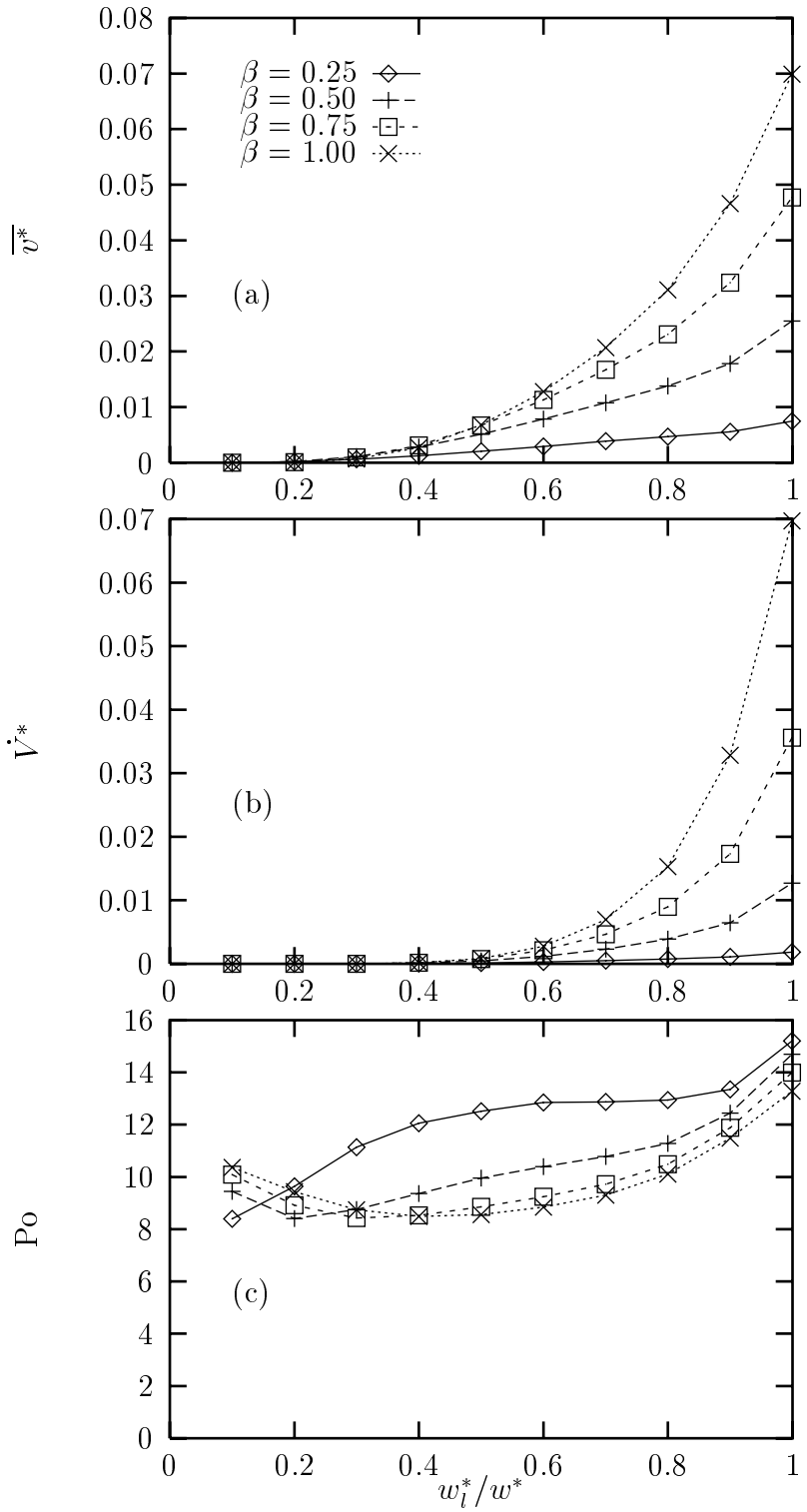

Figure 5: Variation of the flow variables with groove fill ratio for various values of groove aspect ratio ($\tau_{lv}^* = 0.0$, $\phi = 0°$): (a) Mean velocity; (b) Volumetric flow rate; (c) Poiseuille number.

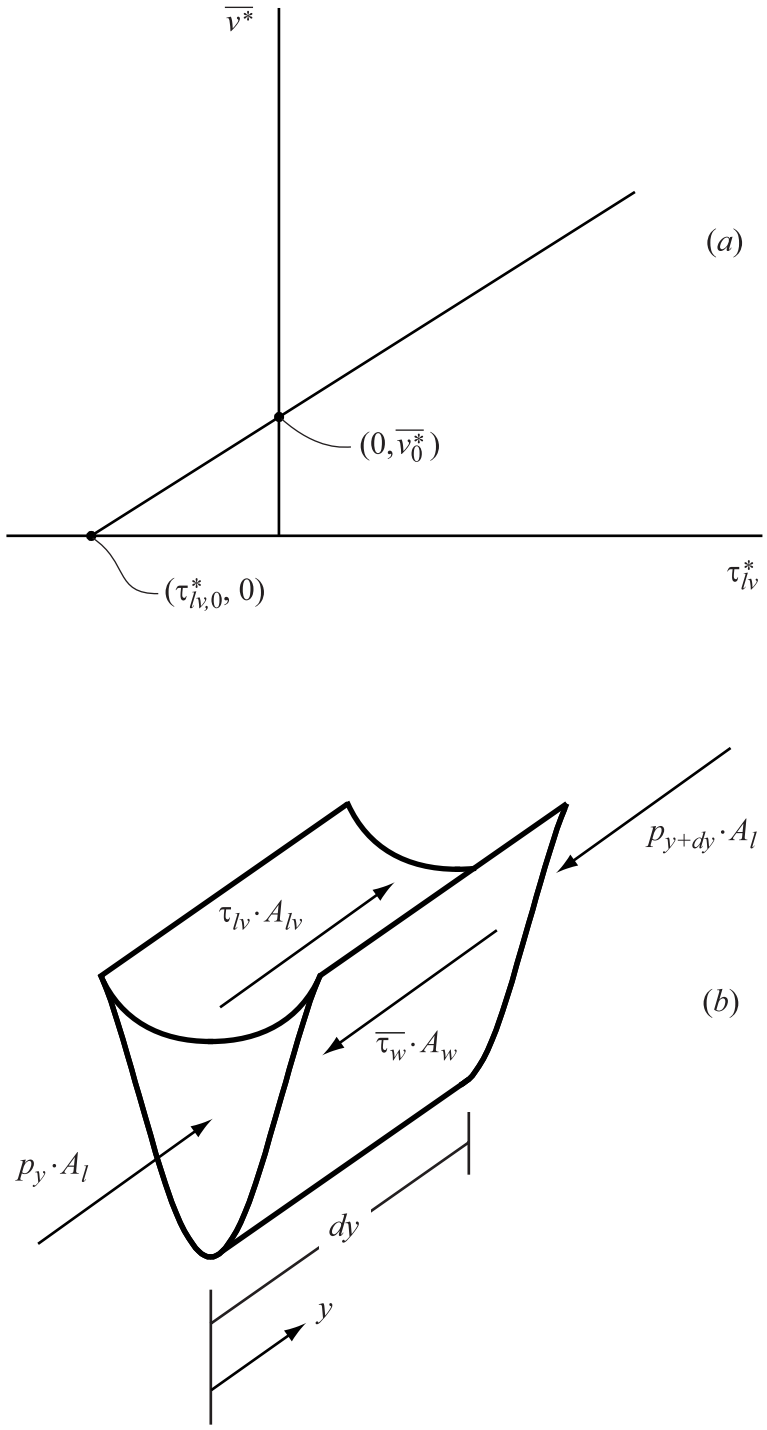

Figure 6: Semi-analytical solution for $\overline{v^*}$: (a) Definition of parameters; (b) Force balance on the liquid in a sinusoidal groove.

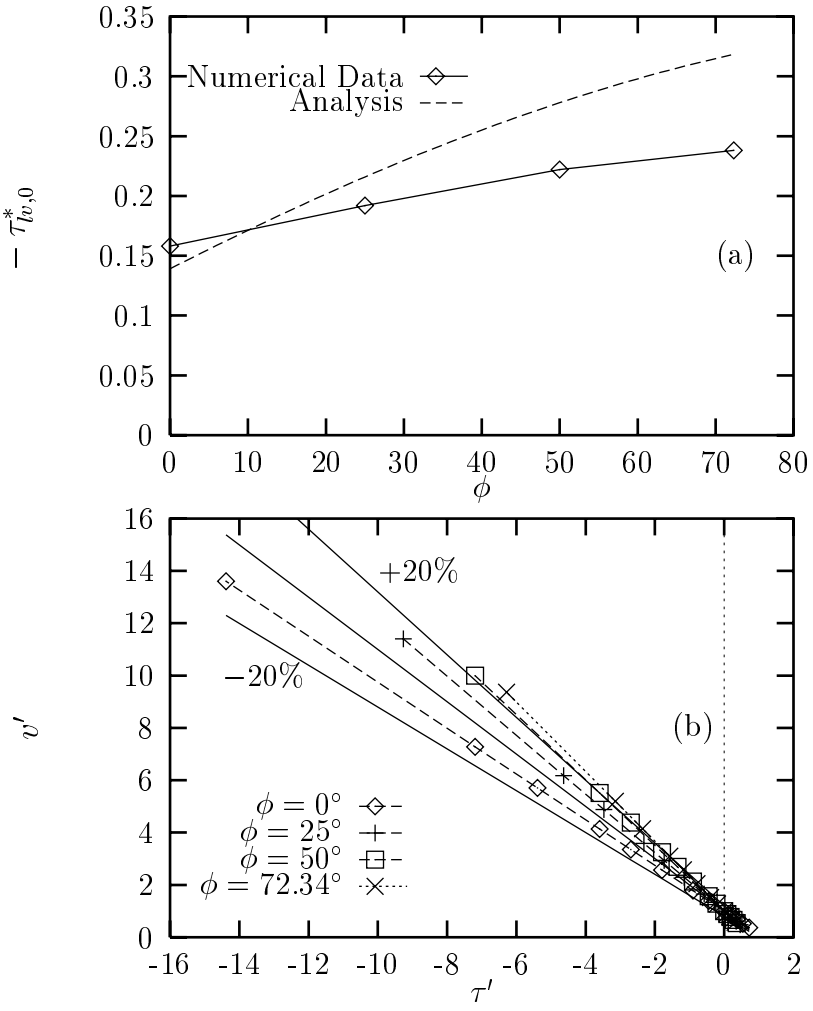

Figure 7: Comparison of the semi-analytical solution with numerical data ($\beta = 0.5$, $w_l^*/2 = 0.25$): (a) Countercurrent vapor shear stress required for $\overline{v^*} = 0$; (b) Normalized mean velocity versus normalized shear stress at the liquid-vapor interface.